IOPscience iopscience.iop.org

Home Search Collections Journals About Contact us My IOPscience

A structural model for the relaxor $PbMg_{1/3}Nb_{2/3}O_3$ at 5 K

This article has been downloaded from IOPscience. Please scroll down to see the full text article.

1991 J. Phys.: Condens. Matter 3 8159

(http://iopscience.iop.org/0953-8984/3/42/011)

View the table of contents for this issue, or go to the journal homepage for more

Download details:
IP Address: 171.66.16.159
The article was downloaded on 12/05/2010 at 10:36

Please note that terms and conditions apply.

J. Phys.: Condens. Matter 3 (1991) 8159–8171. Printed in the UK

A structural model for the relaxor $PbMg_{1/3}Nb_{2/3}O_3$ at 5 K

N de Mathan†, E Husson†‡, G Calvarin†, J R Gavarri§, A W Hewat‖ and A Morell¶

† Laboratoire de Chimie Physique du Solide, Unité de Recherche associée au CNRS 453, Ecole Centrale de Paris 92295, Chatenay-Malabry Cédex, France

‡ Laboratoire de Physique et Mécanique des Matériaux, Ecole Supérieure de l'Energie et des Matériaux, Université d'Orléans et CRPHT-CNRS Orléans, 45071 Orléans Cédex, France

§ Laboratoire des Matériaux à Propriétés Variables, Université de Toulon et du Var, BP 132, 83957 La Garde, France

‖ Institut Laue–Langevin, avenue des Martyrs, 156X, 38042 Grenoble Cédex, France

¶ Thomson-CSF, LCR, Domaine de Corbeville, 91404 Orsay Cédex, France

Received 21 May 1991, in final form 17 June 1991

Abstract. The perovskite structure of the relaxor $PbMg_{1/3}Nb_{2/3}O_3$ (PMN) is studied using x-ray and neutron powder diffraction data. The static diffuse scattering (SDS) observed in the diffraction patterns at low temperatures is interpreted using a two-phase Rietveld analysis. The structural model is based on a long-range structure with an average cubic symmetry, and a short-range order due to atomic shifts involved by the formation of polar regions. The two-phase model provides a good improvement in reliability factors. The correlation length and the coexistence of different phases at low temperatures are discussed.

1. Introduction

The relaxor perovskite oxide $PbMg_{1/3}Nb_{2/3}O_3$ (PMN) exhibits a high value of the dielectric constant over a wide temperature range with a maximum close to $T_{max} = -266$ K for a measurement frequency of 1 kHz. In the low temperature phase of PMN, there are no ferroelectric domains [1] and crystals are optically isotropic [2]. In order to interpret the variations in the refractive index with temperature, Burns and Dacol [3] assumed existence of small polar regions which appear below T_d (T_d is close to 600 K). By Raman spectroscopy, below 300 K, Husson *et al* [4] showed the existence of Nb—O polar bonds similar to the Nb—O bonds found in classical ferroelectric perovskites. This result also suggests the existence of small polar regions at low temperatures. A structural study performed on PMN ceramic samples by x-ray and neutron diffraction between 1000 and 5 K has permitted us to follow the evolution of the diffraction patterns and to propose models for the high- and low-temperature phases of PMN [5].

In this paper, the profiles of the low-temperature diffraction lines are carefully analysed in order to improve the previous structural models.

2. Experimental details

PMN ceramics were prepared according to the process described in [6] and the samples used for this study were powders obtained by crushing sintered ceramics discs and

0953-8984/91/428159 + 13 $03.50 © 1991 IOP Publishing Ltd

annealed in order to reduce the grinding effects. The x-ray powder diffraction patterns were recorded over the angular range $10° < 2\theta < 130°$ on a high-accuracy Microcontrole diffractometer using Cu Kα radiation (graphite monochromator) of a rotating-anode generator of 18 kW. The low-temperature study was performed in a He cryostat with a stability and precision of 0.1 K. The neutron powder diffraction patterns were collected on a D1A diffractometer at the Institut Laue–Langevin, Grenoble, over the angular range $10° < 2\theta < 160°$ in steps of 0.05° (2θ). The wavelength used was 1.3844 Å. The PMN powder was put in a vanadium can. The structural refinements were carried out using the Rietveld profile [7] method with the computer program DBW 3.2 [8].

3. Previous structural results

Between 300 K and 5 K, no splitting of the lines or shoulders indicating a distortion of the cubic cell is observed in the x-ray and neutron diffraction patterns: as the temperature decreases, the full width at half-maximum (FWHM) increases continuously for all the lines (between 6 and 33% depending on the lines). This change in lineshape could result from the growth of polarized small regions, as was also observed in PLZT [9–11]. From a structural point of view, the low-temperature phase remains roughly cubic [5]. However, when the temperature decreases, a careful analysis reveals firstly the progressive appearance of the quasi-extinguished lines of the high-temperature phase, (320), (322)–(410), (331), (421), in the form of broadened weak lines and secondly a continuous widening of the bases of some diffraction lines [5].

Structural refinement calculations have been performed using the Rietveld method with two models, at 5 K.

(i) The first model corresponds to that used to describe the paraelectric high-temperature phase; the symmetry is cubic, with space group Pm3m ($Z = 1$) and atoms are statistically displaced from their special positions. Pb atoms are shifted along the ⟨110⟩ and/or ⟨111⟩ directions. Oxygen atoms are shifted isotropically in two planes parallel to the faces of the cube so that their distribution is disc shaped. The shifts of the Mg/Nb atoms are very small and not precise. Such a model leads to profile and intensity reliability factors $R_{wp} = 11\%$ and $R_B = 4\%$, respectively [5].

(ii) The second model corresponds to that found in the rhombohedral phase of $KNbO_3$ (R3m space group). The symmetry is polar and there is no disorder in the atomic positions. In this case, the reliability factors are $R_{wp} = 22\%$ and $R_B = 12\%$.

So, the first model seems to fit the experimental data better than the second model does but the R-values are not quite satisfactory as the widening observed at the bases of some diffraction lines is not taken into account.

4. A new model for the low-temperature phase of PMN

4.1. Origin of the diffuse scattering

The diffuse scattering observed may originate from different phenomena.

(i) *Inelastic interactions.* In the neutron diffraction patterns, scattering may be due to inelastic interactions between the neutron beam and the vibrational modes of the crystal but the widening observed in the neutron and x-ray patterns is assumed to have

the same origin. Inelastic interactions have a very weak influence on the x-ray patterns. Again this scattering increases when the temperature decreases.

(ii) *Partially ordered distribution of the Mg and Nb atoms.* In this case, scattering should be localized at the theoretical positions of the superlattice peaks of an ordered structure. On the other hand, if the ordered domains observed by high-resolution electron microscopy [12] were regularly disposed in the space, scattering should be localized beside the Bragg peaks and its intensity should be constant with temperature.

(iii) *Huang's scattering* [13]. This is due to an elastic relaxation of the crystal structure around a defect or an impurity. In PMN, a local distortion of the cubic cell may be assumed, but generally the distortions observed in the ferroelectric phase transitions of perovskites are very weak [14, 15] and they induce very small atomic displacements. Therefore, such an elastic deformation does not seem to be at the origin of the scattering observed in PMN.

(iv) *Correlations of atomic displacements.* They lead also to diffuse scattering. In some conditions, this scattering may be concentrated at the Bragg angles and its intensity increases with increasing diffraction angle. Classical examples of diffuse scattering induced by atomic shifts are thermal diffuse scattering (TDS) [16, 17] or static diffuse scattering (SDS). In the first case, atomic shifts correlated in time and in space are induced by a vibrational mode. TDS leads to widening at the bases of some diffraction lines. In the last case, the effects on diffraction profiles are the same but the evolution with temperature is fully different.

Taking into account the decrease in the diffuse scattering as the temperature increases, the latter hypothesis (SDS) seems to be the most probable; a strong displacement disorder exists in PMN and correlations of static atomic shifts may locally occur and induce the observed scattering.

4.2. *Existence of local polarization*

The strong displacement disorder of all the atoms, pointed out by Bonneau *et al* [5, 18], could not be related to the ferroelectric behaviour of the PMN; for example, the Pb^{2+} cations, from their chemical nature, i.e. their lone pair, cannot lie on the special positions of the perovskite structure, even at high temperatures, which is actually observed. In the same way, an important average displacement of cations in octahedral sites is observed at high temperatures. The appearance of progressive widening at the basis of diffraction lines when the temperature decreases seems to be related to the ferroelectric properties of PMN. This is confirmed by much experimental evidence which indicates the existence of local polarization for the low-temperature phase of the relaxors [3, 4]. Again, the appearance of polarization is necessarily related to an atomic rearrangement, i.e. to a local polar symmetry.

Describing the structure through a cubic symmetry implies that no polarization exists. When, for example, a Nb^{5+} cation is displaced along a [111] direction, it lies off its special position and seven other equivalent positions are generated [19]. The cation occupies statistically the eight positions so far as there is no correlation in the disordered positions; the Nb^{5+} disordered position in the nth cell is independent of the Nb^{5+} disordered position in the $(n + 1)$th cell. In these conditions, the average position of the Nb atoms is a special position (centre of the cube) and no spontaneous polarization appears in the crystal.

If spontaneous polarization exists, the structure is described by a polar space group, e.g. R3m. Thus, when a Nb^{5+} cation is shifted from the centre of the cube along the [111] direction (rhombohedral axis), it remains in a special position. If in a domain, all the Nb^{5+} are shifted in the same manner, a spontaneous polarization is induced after the cubic → polar symmetry transition. This symmetry change involves the existence of a correlation of the atomic shifts.

In the proposed model, a unique local polarization appears in very small domains and no global polarization exists in the crystal. So, it is necessary to separate the short- or medium-range order and the long-range order effects. At short or medium range, the local symmetry is polar, and the atomic shifts are correlated. At long range, the local polarization of the crystal varies from place to place so that no global polarization exists. Atomic displacements are not correlated; atoms statistically lie on disordered positions; so, the average symmetry is cubic. The small polar regions are considered to be included in the host lattice and not independent of it; the structure of a polar region differs from that of the host lattice only in the atomic shifts and the scattering of the polar region is partially coherent with that of the cubic host lattice. Thus, the crystal does not behave as a polar homogeneous crystal, because the coherence length of the polar zones is spatially limited, nor does it behave as a perfectly cubic crystal because of the strong deviations from the cubic symmetry. The crystal is neither cubic nor polar and a classical treatment is not sufficient. A more detailed intensity calculation is then necessary.

4.3. Scattering intensity calculation

One considers that an atom of the nth cell is shifted by $\boldsymbol{d}_n$ from its special position. The structure factor F_n of this cell depends on $\boldsymbol{d}_n$ which varies from one cell to another. There are two ways to take atomic shifts into account.

(i) A treatment of TDS or SDS type can be used; atomic shifts are supposed to be small. The structure factor F_n may be described as a perturbation of the structure factor F_0 of an ideal structure where atoms are not shifted:

$$F_n = F_0 \exp(i\boldsymbol{k} \cdot \boldsymbol{d}_n)$$

where $\boldsymbol{k}$ is the scattering vector.

(ii) When atomic shifts are quite strong as in PMN, the structure factor F_n may be described as a perturbation of the average structure factor F_{av} corresponding to an average cell in which atoms are randomly displaced [13, 16, 17, 20]. F_{av} is defined as follows:

$$F_{av} = (1/N)\left(\sum_n F_n\right)$$

where the summation is made on the N cells of the crystal. If a correlation of atomic shifts exists, two neighbouring cells are assumed to have the same structure factor. This leads to a locally polarized structure for which the structure factor is called F_{pol}. The notions of 'neighbouring' and 'distant' cells depend on the correlation length. Thus F_{av} is the structure factor of the long-range structure, which may also represent the high-temperature paraelectric phase, whereas F_{pol} is the structure factor of the local structure, which characterizes an ordered polar crystal. F_{pol} may have as many values as existing polarization directions; that is, for a rhombohedral symmetry, F_{pol} may take eight different values. In this description, the crystal is made of polarized cells in which the

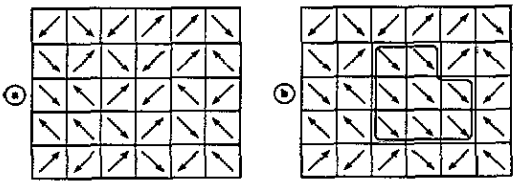

Figure 1. (*a*) Fully disordered polarized cells of the high-temperature phase. (*b*) Existence of correlations of the atomic displacements at short range (nanodomains) in the low-temperature phase.

polar direction is correlated at short-range but varies from place to place in the crystal at long-range (figure 1). Thus, the scattering intensity, in the k-direction, may be decomposed into two components (see appendix):

$$I = I_{\text{Bragg}} + I_{\text{sds}}.$$

The first component is defined as

$$I_{\text{Bragg}} = (F_{\text{av}})^2 \exp\{\mathrm{i}\boldsymbol{k} \cdot \boldsymbol{r}_{pp'}\}$$

where $r_{pp'}$ is the vector between two p and p' cells. The summation is made over all the cells. The diffraction lines are sharp and their intensity is proportional to F_{av}^2. The second component is defined as

$$I_{\text{sds}} = (F_{\text{pol}} - F_{\text{av}})^2 \exp\{\mathrm{i}\boldsymbol{k} \cdot \boldsymbol{r}_{nn'}\}.$$

This term corresponds to the existence of a correlation; the summation (nn') is made over the neighbouring cells. The diffraction lines are widened by size effects and their intensities are proportional to $(F_{\text{pol}} - F_{\text{av}})^2$ terms. These two scattering components are located at the same Bragg angle. They are independent and can be added. So, the appearance of a correlation can be observed on the profile of the lines, in so far as the diffuse scattering related to this correlation appears as a very broad and weak line, i.e. as a tail of the Bragg peak corresponding to the average network diffraction. The structure factor F_{av} and the intensity I_{Bragg} describe the high-temperature structure of PMN. The transition between this structure and the low-temperature structure is treated as a perturbation with the introduction of a second intensity I_{sds}.

5. Results

In order to verify the validity of the proposed model, structural refinement calculations have been performed:

(i) with only one component (I_{Bragg}) using a classical refinement;
(ii) with two components ($I_{\text{Bragg}} + I_{\text{sds}}$).

5.1. Choice of a structure for the low-temperature short-range order

It is necessary to define the local polar structure, i.e. the type of symmetry and the types of atomic shift chosen for the model. Very little has been published about the symmetry of the low-temperature phase of PMN. By x-ray diffraction on a single crystal, Shebanov *et al* [21] observed a rhombohedral structure at low temperatures. Hysteresis loops on a PMN single crystal reported by Schmidt *et al* [22] show that polarization is much weaker

along a ⟨100⟩ direction than along a ⟨110⟩ or a ⟨111⟩ direction. On the other hand, Bonneau *et al* [5] showed that the ⟨100⟩ directions of atomic shifts are not probable. Thus, the hypothesis of a tetragonal symmetry seems to be excluded. Therefore, a rhombohedral symmetry was firstly considered. The space group R3m found in the low-temperature phases of $KNbO_3$ and $BaTiO_3$ [14, 15] was chosen; it involves antiparallel shifts of cations (Pb, Mg/Nb) against oxygen atoms along the [111] rhombohedral axis. Thus, the model used was the following: at long range, in the average cubic structure, each atom occupies eight disordered positions shifted from the symmetry site along the eight ⟨111⟩ directions; at short range, in the rhombohedral polar structure, each atom occupies just one of these displaced positions (figure 1).

5.2. *Refinement of the structure at 5 K*

The refinement calculations were performed using

(i) only one component (I_{Bragg}) which corresponds to a classical Rietveld method and
(ii) two components ($I_{Bragg} + I_{sds}$).

The first component I_{Bragg} corresponds to the average cubic structure. The second component I_{sds} is obtained as follows: in a same crystal, the atoms are put

(i) on the polar positions with a positive scattering factor and
(ii) on the disordered positions of the average cubic structure with a negative scattering factor, which allows us to take the intensity $I_{sds} = (F_{av} - F_{pol})^2 \exp(i\boldsymbol{k} \cdot \boldsymbol{r}_{nn'})$ into account.

This second intensity calculation is just an artifice; it does not correspond to a real crystal and it is proportional to $(F_{av} - F_{pol})^2$. In fact, theoretically, F_{pol} may take different values following the orientation of the region polarization. In order to obtain a correct estimation of the diffused intensity in the $[hkl]$ direction, it is necessary to calculate the average intensity $[F_{av}(hkl) - F_{pol}(hkl)]^2$ for the different possible orientations of the polarization. This is performed directly by a program which calculates a total intensity for the different reflections of an $\{hkl\}$ family.

Most of the refined parameters are common to the two components:

(i) atomic shift values;
(ii) cell parameter;
(iii) zero of the goniometer;
(iv) asymmetry parameter;
(v) profile functions: a pseudo-Voigt function for x-ray lines and a Gaussian function for neutron diffraction lines have been chosen.

In addition, there are the following:

(vi) the scale factors (one for each component);
(vii) the FWHM parameters U, V, W (three for each component) defined as follows: $H_k^2 = U\tan^2(\theta_k) + V\tan(\theta_k) + W$ where H_k is the FWHM of the k line.

So, it can be observed that the introduction of a second component involves only four extra parameters (16 instead of 12); therefore the model is very simple.

Table 1. Results of the powder x-ray and neutron diffraction refinements of PMN at 5 K.

		Two components		One component	
		X-ray	Neutrons	X-ray	Neutrons
Cell parameter	a (Å)	4.0488	4.0278	4.0488	4.0278
Atomic shifts (Å)	d_{Pb}	0.36 ± 0.001	0.35 ± 0.002	0.29 ± 0.001	0.35 ± 0.002
	$d_{Mg/Nb}$	0.10 ± 0.005	0.09 ± 0.004	0.18 ± 0.005	0.0
	d_{1O}[a]	0.17	0.17 ± 0.001	0.17	0.18 ± 0.002
	d_{2O}	0.08	0.08 ± 0.003	0.08	0.08 ± 0.001
Debye–Waller factors* (Å²)	B_{Pb}	0.33	0.33	0.33	0.33
	$B_{Mg/Nb}$	0.15	0.15	0.15	0.15
	B_O	0.24	0.24	0.24	0.24
Profile parameters	g	0.893	—	1.075	—
First component	S_1	0.3780×10^{-5}	0.2911×10^{-2}	0.4060×10^{-5}	0.3008×10^{-2}
	U_1	0.018 12	0.167 94	0.040 75	0.184 04
	V_1	−0.003 82	−0.511 25	−0.017 58	−0.542 81
	W_1	0.004 79	0.470 41	0.006 50	0.492 42
Second component	S_2	0.3136×10^{-5}	0.1778×10^{-2}		
	U_2	1.074 24	1.549 05		
	V_2	−0.929 04	−2.659 98		
	W_2	0.597 22	2.111 30		
Reliability factors (%)	R_{wp}[b]	10.1	7.8	14.6	12.6
	R_p[c]	7.4	11.4	9.6	5.6
	R_{Bragg1}[d]	3.4	2.2	4.05	4.8
	R_{Bragg2}	2.4	2.0		

* Not refined. The values of [5] were used.

[a] d_{1O}: oxygen shifts in the planes parallel to the faces of the cube; d_{2O}: oxygen shifts along directions perpendicular to the faces.

[b] Weighted profile $R_{wp} = 100[\Sigma\, w(Y_{obs} - Y_{calc})^2/(\Sigma\, wY_{obs}^2)]^{1/2}$.

[c] Profile $R_p = 100\Sigma(Y_{obs} - Y_{calc})/\Sigma Y_{obs}$.

[d] Bragg $R_B = 100\Sigma(I_{obs} - I_{calc})/\Sigma I_{obs}$ for the first and second component. I_{obs}, I_{calc}, observed and calculated integrated intensities; w, weight allocated to each data point.

The results are given in table 1. The two refinement methods can be compared.

(i) The atomic shifts of the B cations exhibit a sensible modification; with the one-component refinement, their average positions cannot be accurately determined [5] and, with the two-component refinement, $d_{Mg/Nb}$ is equal to 0.09 Å.

(ii) The two-component refinement provides good agreement between the atomic positions refined from both x-ray and neutron diffraction data.

(iii) The reliability factors are significantly improved with the two-component refinement and correct values are obtained.

The comparison of the experimental and calculated profiles obtained by the two refinement techniques is particularly interesting; the full profiles of the lines presenting significant widening at their bases, which were not fitted by the one-component technique, are quite satisfactorily fitted by the two-component technique. In addition,

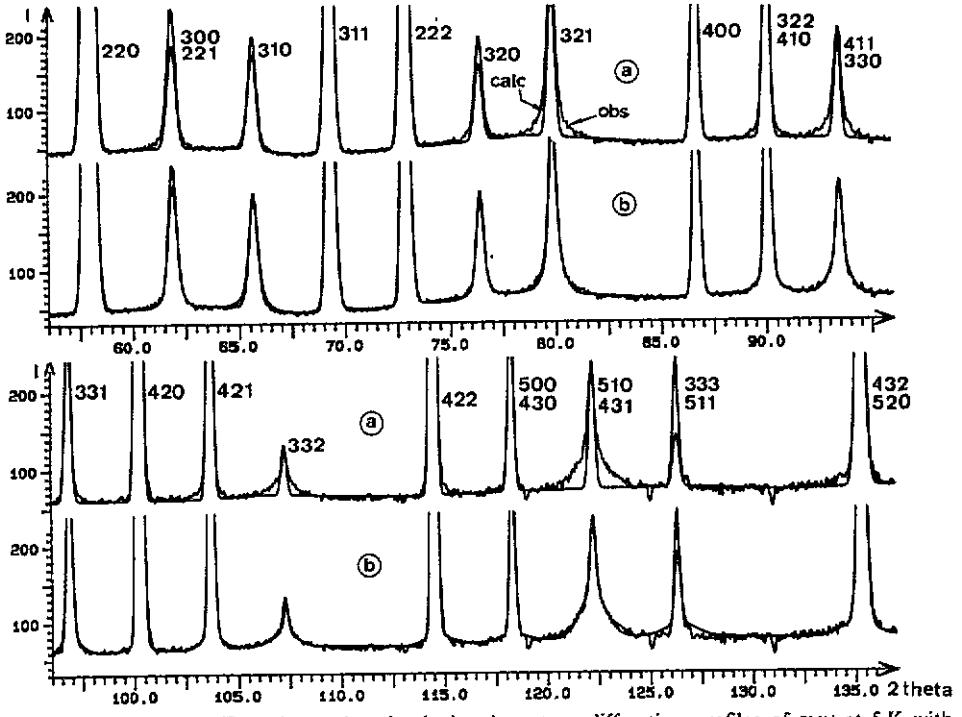

Figure 2. Experimental and calculated neutron diffraction profiles of PMN at 5 K with structural refinement using (*a*) the one-component technique and (*b*) the two-components technique.

the profiles of the unmodified lines are also quite well fitted. This is true for the neutron and the x-ray diffraction data, as shown for a number of diffraction lines in figures 2 and 3.

A calculation has been performed in the same manner with an orthorhombic symmetry (space group, Amm2). The reliability factor R_{wp} is slightly greater ($R_{wp} = 8.11\%$) than for rhombohedral symmetry ($R_{wp} = 7.8\%$) for neutron diffraction data.

The retained rhombohedral structure of the locally short-range polar order is given in figure 4.

6. Discussion

6.1. Description of the short-range polar order

From the above results, the low-temperature phase of PMN seems to be well supported by a short-range polar order model, but the refinement results present some limitations owing to the simplicity of the model.

(i) Calculations show that orthorhombic symmetry is as probable as rhombohedral symmetry. The main feature to be noted is the relative atomic shifts, i.e. antiparallel shifts of Pb and Mg/Nb cations against the oxygen atoms along a [111] (or a [110]) axis. Moreover, because of the high inhomogeneity of the PMN, it is not excluded that other types of correlation could exist at low temperatures.

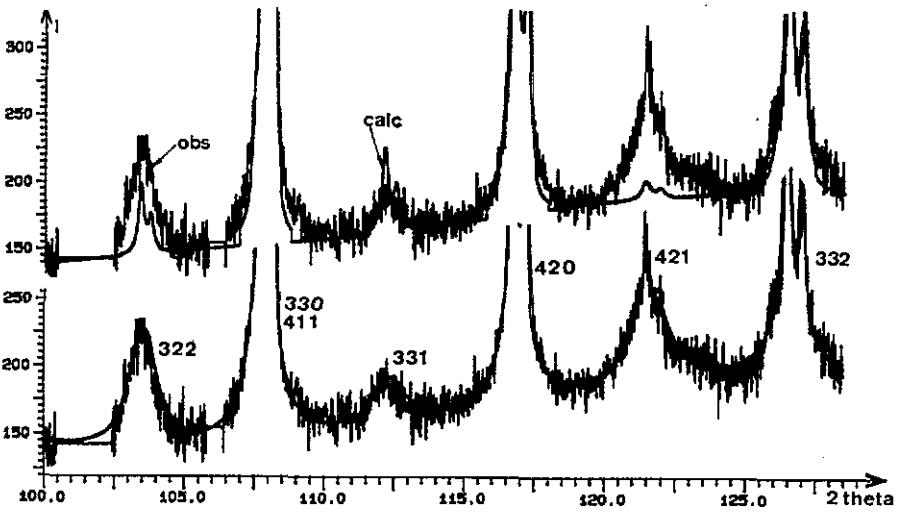

Figure 3. Experimental and calculated x-ray diffraction profiles of PMN at 5 K with structural refinement using (*a*) the one-component technique; and (*b*) the two-components technique.

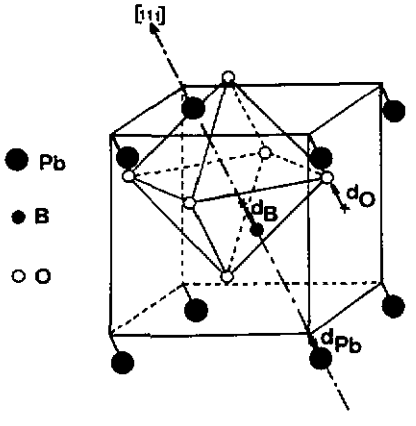

Figure 4. Rhombohedral structure of the locally polar nanoregions at 5 K.

(ii) The distribution of the Mg and Nb atoms on the B site of the perovskite has been considered as fully disordered in the calculations. However, it is known that nanodomains with a 1–1 B-site ordering exist in PMN [12, 23]. The MgO_6 and NbO_6 octahedra, which are chemically different, may play different roles in the polar domains.

6.2. Polar correlation nature

The polar correlation is not characterized only by the atomic shifts. One can also determine the polar 'phase' amount and the correlation length.

6.2.1. Polar phase amount. The existence of nanopolar regions induces the presence of at least two local phases. This fact may be illustrated by two images.

(i) The crystal is made of islands of polar ordered nanodomains (first phase) immersed inside a disordered paraelectric host lattice (second phase).

(ii) The crystal is made of a pavement of polar nanodomains (first phase). Taking into account that the interdomain regions may be more important than the domain size, the interdomain volume cannot be neglected (second phase).

In the two cases, the crystal is not of a single-phase nature. It should be interesting to evaluate the amount of crystal affected by the polar order. An approximation of this may be deduced from the scale factors S_1 and S_2 of each component of the refinement calculations (table 1). If a given structure is described in cubic symmetry and in rhombohedral symmetry, the scale factors are different: because of the multiplicity of the reflections, which are different for the two symmetries, a scale factor $S = 1$ in cubic symmetry corresponds to $S = 4$ in rhombohedral symmetry. If the calculated factor S_2 is divided by 4, the relative ratios $r = S_2/4S_1$ for x-ray and neutron diffraction data lead, respectively, to $r = 20\%$ and $r = 15\%$. These values are only approximate. However, they give an order of magnitude of the polar phase amount at 5 K. Thus, the polar structure does not seem to occupy the whole space.

6.2.2. Polar nanoregions. The length of the polar correlation may be deduced from our results; the diffraction lines of very small crystals are widened by a size effect according to the Scherrer formula. From x-ray and neutron diffraction data, it is possible to evaluate the correlation length to be about 100 Å at 5 K.

So, zones of about 100 Å exist in the crystal, in which the average polarization is different from zero; they are polar nanoregions. However, the polarization intensity may vary in these nanoregions and the polar direction may differ from one polar region to another. The average polarization of the crystal (or grain) is zero.

Moreover, a spatial isotropic correlation of the atomic shifts has been considered, but the real shape of the polar nanodomains could be discussed; in a recent study on a PZT single crystal with a low titanium content, Rodeler and Kugel [24] show that polar microregions may adopt a cigar form.

Finally, it may be supposed that polarization is not constant in a nanodomain and that domain walls between the nanodomains are not sharp; for example, it can be assumed that a relaxation phenomenon of the polarization occurs around a defect, i.e. the high polarization near the defect decays with increasing distance from the defect.

6.3. Intensity of the diffuse scattering

In a previous study [1], two types of Bragg peak were distinguished in neutron diffraction patterns: ones in which all three indices have the same parity and exhibit no widening at their bases (type I); others in which widening is exhibited at their bases (type II). This observation was related to the expressions for the structure factors; type I lines had a large contribution from the oxygen atom structure factor. As the two Bragg peak families were not clearly observed in the x-ray diffraction patterns (where oxygen atoms have small contributions and Pb atoms a very high contribution), it was concluded that the scattering observed at the bases of the lines was mainly due to the cations and more particularly to the Mg/Nb cations.

Attempts at structural refinement considering correlations between the shifts of only Mg/Nb cations or only Pb cations or Mg/Nb and Pb cations give inconsistent results. Among the trials involving all the atomic shifts, only the solution with antiparallel displacements of cations against oxygen atoms gives satisfactory results.

Table 2. Calculated intensities of the two components for some neutron diffraction lines.

Line	I_1†	I_2‡	I_2/I_1
221–300	26.0	3.6	0.14
310	15.0	4.2	0.28
311	82.0	1.3	0.02
222	94.0	0.7	0.01
320	18.0	2.7	0.16
321	26.0	8.5	0.33
400	47.0	0.0	0.0
322–410	8.0	1.2	0.15

† I_1 = first-component intensity.
‡ I_2 = second-component intensity (arbitrary units).

In table 2, the calculated intensities for some neutron diffraction lines are reported; the first-component intensity corresponds to the average structure and thus to sharp lines, whereas the second-component intensity corresponds to the polar regions and thus to widening of the bases. The intensity ratio of both components is very weak for lines of type I, which is in agreement with the experimental observations and also confirms the chosen model.

For the polar structure (second component), the calculation shows that in the expression for the diffuse intensity $I_{sds} = (F_{av} - F_{pol})^2$, only the imaginary part of F_{pol} is preponderant. Thus, an approximate calculation of I_{sds} gives, for a type I line,

$$I_{sds} = \{b_{Pb} \sin[(h + k + l)\, z_{Pb}] \pm b_{Mg/Nb} \sin[(h + k + l)\, z_{Mg/Nb}] - 3b_O \sin[(h + k + l)\, z_O]\}^2$$

and, for a type II line,

$$I_{sds} = \{b_{Pb} \sin[(h + k + l)\, z_{Pb}] \pm b_{Mg/Nb} \sin[(h + k + l)\, z_{Mg/Nb}] + b_O \sin[(h + k + l)\, z_O]\}^2$$

with $z_{Pb} = 0.56$, $z_{Mg/Nb} = 0.14$ and $z_O = 0.29$ ($z_A = 2\pi d_A/a$, where a is the cell parameter) and with $b_{Pb} = 0.96$ ($\times 10^{-12}$ cm), $b_{Mg} = 0.54$ ($\times 10^{-12}$ cm), $b_{Nb} = 0.69$ ($\times 10^{-12}$ cm) and $b_O = 0.58$ ($\times 10^{-12}$ cm).

For type I lines, the oxygen contribution is subtracted from the cation contribution and thus I_{sds} is very small but, for the type II lines, the contributions are added and thus I_{sds} has a considerable value.

For x-ray diffraction data, the atomic scattering factors and the observed phenomena are different. The lines which exhibit the most important widening are those with two even indices (figure 3).

7. Conclusion

This work permitted us to describe the low-temperature phase of PMN at 5 K. The widening observed at the bases of some x-ray and neutron diffraction lines are interpreted as scattering induced by atomic shift correlations, leading to a locally polar structure. The results obtained by the two techniques are in good agreement. The proposed model

gives a very good fit between the calculated and experimental patterns, particularly at the line bases, which confirms the validity of the model. The locally polar structure should be close to the polar structures of classical ferroelectrics such as $BaTiO_3$ or $KNbO_3$ and should be characterized by antiparallel shifts of the cations against oxygen atoms inducing a dipolar moment. In our model, the local symmetry is assumed to be rhombohedral, with atomic shifts along the [111] direction of the cube, i.e. the rhombohedral axis. The correlation length of the polar regions increases when the temperature is lowered and has been evaluated to be about 100 Å at 5 K; local polarization variations surely exist in the material and two phases seem to coexist in the crystal at 5 K: a polar phase which has been roughly evaluated at 20% and a non-polar phase associated with host lattice.

Appendix

The coherent scattered intensity in the k-direction may be decomposed in the sum of four terms:

$$I = \sum_{pp'} [F_p F_{p'} \exp(i\boldsymbol{k} \cdot \boldsymbol{r}_{pp'})] \qquad \text{summation of the whole crystal}$$

$$I = \sum_{pp'} [(F_{av} + f_p)(F_{av} + f_{p'}) \exp(i\boldsymbol{k} \cdot \boldsymbol{r}_{pp'})]$$

$$I = I_1 + I_2 + I_3 + I_4$$

$$I_1 = \sum_{pp'} [(F_{av})^2 \exp(i\boldsymbol{k} \cdot \boldsymbol{r}_{pp'})]$$

$$I_2 = \sum_{pp'} [(F_{av} f_{p'}) \exp(i\boldsymbol{k} \cdot \boldsymbol{r}_{pp'})]$$

$$I_3 = \sum_{pp'} [(f_p F_{av}) \exp(i\boldsymbol{k} \cdot \boldsymbol{r}_{pp'})]$$

$$I_4 = \sum_{pp'} [(f_p f_{p'}) \exp(i\boldsymbol{k} \cdot \boldsymbol{r}_{pp'})].$$

The first contribution I_1 refers to all cells and produces therefore sharp reflections with intensity proportional to F_{av}^2:

$$I_{Bragg} = I_1 = F_{av}^2 \sum \exp(i\boldsymbol{k} \cdot \boldsymbol{r}_{pp'})].$$

By an index change, it is seen that $I_2 = I_3 = 0$:

$$I_2 = F_{av} \sum_p \sum_{p'} f_{p'} \exp(i\boldsymbol{k} \cdot \boldsymbol{r}_{pp'})$$

$$I_2 = F_{av} \left(\sum_{p''} \exp(i\boldsymbol{k} \cdot \boldsymbol{r}_{pp''}) \right) \left(\sum_{p'} f_{p'} \right)$$

$$I_2 = F_{av} \left(\sum_{p''} \exp(i\boldsymbol{k} \cdot \boldsymbol{r}_{p''}) \right) 0$$

$$I_2 = 0.$$

The I_4 term is

$$I_4 = \sum_p \sum_{p'} f_p f_{p'} \exp(i\boldsymbol{k} \cdot \boldsymbol{r}_{pp'}).$$

If the p and p' cells are distant cells, there is no correlation between f_p and $f_{p'}$ and their contribution may be neglected. On the contrary, if the p and p' cells are neighbouring cells, there is a correlation of the atomic shifts so that $f_p = f_{p'}$. The neighbouring cells thus contribute to the interferences in a constructive manner:

$$I_4 = (fp)^2 \sum_{p,p'} \exp(i\boldsymbol{k} \cdot \boldsymbol{r}_{pp'})$$

$$I_4 = (F_{av} - F_{pol})^2 \sum_{p,p'} \exp(i\boldsymbol{k} \cdot \boldsymbol{r}_{pp'}).$$

Acknowledgment

The authors would like to thank the French Ministry of Research and Technology (MRT) for financial support.

References

[1] Hilton A D, Randall C A, Barber D J and Shrout T R 1989 *Ferroelectrics* **89** 379
[2] Setter N and Cross L E 1981 *Ferroelectrics* **37** 551
[3] Burns G and Dacol F H 1983 *Phys. Rev.* B **28** 2527
[4] Husson E, Abello L and Morell A 1990 *Mater. Res. Bull.* **25** 539
[5] Bonneau P, Garnier P, Calvarin G, Husson E, Gavarri J R, Hewat A W and Morell A 1991 *J. Solid State Chem.* **91** 350
[6] Swartz S L and Shrout T R 1982 *Mater. Res. Bull.* **17** 1245
[7] Rietveld H M 1969 *J. Appl. Crystallogr.* **2** 65
[8] Wiles D B and Young R A 1981 *J. Appl. Crystallogr.* **14** 149
[9] Darlington C N W 1989 *Phys. Status Solidi* a **113** 63
[10] Darlington C N W 1988 *J. Phys. C: Solid State Phys.* **21** 3851
[11] Darlington C N W and Cernik R J 1989 *J. Phys.: Condens. Matter* **1** 6019
[12] Husson E, Chubb M and Morell A 1989 *Mater. Res. Bull.* **24** 201
[13] Cohen J B 1966 *Diffraction Methods in Materials Science* (London: Macmillan) p 297
[14] Hewat A W 1974 *Ferroelectrics* **6** 215
[15] Hewat A W 1973 *J. Phys. C: Solid State Phys.* **6** 2559
[16] Guinier A 1964 *Théorie et Technique de la Radiocristallographie* (Paris: Dunod) p 531
[17] Cowley J M 1966 *Diffraction Physics* (Amsterdam: North-Holland) p 254
[18] Bonneau P, Garnier P, Husson E and Morell A 1988 *Mater. Res. Bull.* **24** 357
[19] Comès R, Lambert M and Guinier A 1970 *Acta Crystallogr.* A **26** 244
[20] Boysen H, Frey F and Jagodzinski H 1984 *Rigaku J.* **1** 3
[21] Shebanov L A, Kapostins P P and Zvirgzds J A 1984 *Ferroelectrics* **56** 53
[22] Schmidt G, Arndt H, Borchhardt G, von Cieminski J, Petzsche T, Borman K, Steinberg A, Zirnite A and Isupov V A 1981 *Phys. Status Solidi* a **63** 501
[23] Chen J, Chan H M and Harmer M P 1989 *J. Am. Ceram. Soc.* **72** 593
[24] Rodeler K and Kugel G E 1990 *Ferroelectrics* **106** 287